International Journal of Thermofluids 27 (2025) 101239

Contents lists available at ScienceDirect

International Journal of Thermofluids

journal homepage: www.sciencedirect.com/journal/international-journal-of-thermofluids

A review of the recent advances in heat transfer through ducting in the rotational moulding process and the future trends

Sutirtha Chowdhury [a,b], Jayantha Epaarachchi [a,b], Ahmad Sharifian-Barforoush [a], Md Mainul Islam [a,b,*]

[a] School of Engineering, University of Southern Queensland, Toowoomba, QLD 4350, Australia
[b] Centre for Future Materials & Institute of Advanced Engineering and Space Sciences, University of Southern Queensland, Toowoomba, Australia

ARTICLE INFO

Keywords:
Rotational moulding
Convection
Mould area enhancement
Cycle time reduction
Pressure drop
Air flow rate
Near-wall treatment
Insulation
Carbon emission

ABSTRACT

A common technique for producing large-scale hollow plastic items is rotomoulding. Rotation speed, mould design, and temperature management significantly affect the quality of finished products. A production peak in the rotomoulding business is imminent due to the increasing demand. Though theoretical and experimental data from the previous studies regarding rotational moulding validate their hypothesis but lack of information about practical usage while production time evolves questions about the accuracy and efficiency of innovations. Meanwhile, the lack of sufficient research on the phase transition from the heat source for the rotomoulding procedure led to a great research gap in this field. Nevertheless, conclusions are of substantial value to the subject matter; however, previous studies cannot be regarded as precise in the analysis. Consequently, the review paper sought to emphasise the increasing challenges, such as temperature variation, air leakage, pressure drop, and improved heat distribution techniques. The first phase of the paper involves a discussion and analysis of research findings from the previous decade. The enhancement of the mould area is being proposed based on previous findings to improve heat efficiency. In the second phase, the authors aimed to provide insights into enhancing heat transfer within the ducting system of a rotomoulding oven by exploring duct designs, implementing FADS, and optimising insulation techniques, all while minimising carbon emissions in the process. In addition, the cost-effectiveness of ducted ovens, enhanced insulation processes, and the selection of insulation materials based on oven configuration will yield benefits for rotomoulders in the near future. The authors presented the economic advantages of installing an appropriate ducting system in a rotational moulding machine oven, demonstrating a net annual savings of 12.7 % and a short payback period for an additional investment.

1. Introduction

A Rotational Moulding, often known as the rotomoulding process is a method to fabricate hollow plastic products. This process is suitable for manufacturing hollow plastic products with complex in design, shape, size and precise surface texture [1]. The high-quality products rely on critical parameters like heating, melting, and cooling of the raw material and the rotational speed of the mould. The rotational moulding process has gained popularity in the last two decades in producing hollow seamless products [2–4] such as large container tanks. Rotational moulding processes are mostly renowned for making tanks (Industrial or Agricultural) using HDPE (High-density polyethylene) and LLDPE (Linear low-density polyethylene). Polyethylene (PE) is a widely used material in the process for its versatile characteristics and properties such as high rigidity, flexibility, high tensile strength and impact resistance. Existing research works do not consider the importance of heat transfer through ducting systems that are used in rotational moulding. The global market for rotational moulding machines, which was projected to reach US$ 918.7 million in 2023, has not seen enough discussion of the technique to predict significant growth shortly. The market is anticipated to grow at a compound annual growth rate (CAGR) of 3.7 % from 2023 to 2033, reaching US$ 1321 million. The international packaging machinery market, estimated to be worth US$60.91 billion in 2022, was dominated by 1 % to 2 % by rotational moulding machines [5].

Heating a charged mould at a constant temperature during the RM process is considered the most critical setting. Achieving stability of the

* Corresponding author.
E-mail addresses: Sutirtha.Chowdhury@unisq.edu.au (S. Chowdhury), Jayantha.Epaarachchi@unisq.edu.au (J. Epaarachchi), Ahmad.Sharifian-Barforoush@unisq.edu.au (A. Sharifian-Barforoush), Mainul.Islam@unisq.edu.au (M.M. Islam).

https://doi.org/10.1016/j.ijft.2025.101239

Available online 5 May 2025

Nomenclature

Latin Symbol

n_{min}	Minimum speed (1/s)/(rpm)
g	Acceleration of gravity [m/s^2]
r	Tube radius [m]
T	Temperature, K
t	Time, s
ρ	Density, kg/m^3
h_t	Total enthalpy, J/kg
C_p	Specific heat [J.kg^{-1}.k^{-1}]
k	Thermal conductivity [W/(m.k)]
h	Convection heat transfer coefficient [W/m^{2}K]
υ	velocity in air [m/s]
u_T	Shear stress velocity [m/s]
$\bar{u}$	Average speed [m/s]

Dimensionless

y^+	Dimensionless wall distance
Re	Reynolds number
Nu	Nusselt number
Gr	Grashof number
B, C	Constant

Greek symbol

ε	Turbulent dissipation rate (kg/m-s)
ω	Specific rate of dissipation (kg/m-s)

Subscript

z	Coordinate of the surface

required high temperature at atmospheric air in a melting stage is the major challenge in the rotational moulding process. Polypropylene (PP) exhibits more thermal instability compared to polyethylene (PE). Since the flared behaviour in the monomer unit is due to the presence of hydrogen atom (H) and lower reactivity of peroxyl radicals ($PO_2^\bullet$) [6,7] which influences the overall stability and polymer chain formation during the moulding process. Although Sarrabi et al. [8] illustrated the thermal degradation of polypropylene (PP) proposing a model composed of two distinct levels simulating the enthalpy method derived from the thermal transfer mechanism occurring during a processing operation and oxidation mechanism scheme of free additive polymer in the melt state, they have not compared it with polyethylene which is high demand nowadays for industries.

The melting of the plastic coating needs proper heat distribution which will finally result in consistent wall thickness and high-quality product. On the contrary, the cooling process is essential in the process to prevent warping, wrinkles and shrinkage which will result if proper cool air or water is not being directed to the mould. All the process comes under the thermal control system technique, which can be performed within a proper ducting system. Long ducts of temperature distribution latency have a dynamic difficulty. Process delay occurs due to the time it takes for the fluid to travel along the ducts. Table 1 gives an overview of the last decade's research focus on the rotomoulding process and heat transportation in ducts.

Gerardo et al. [9] gave a general solution to a single duct's dynamic problem with time-dependent inlet and ambient temperatures. Periodic heating time was calculated in the model correlating the effect of the thermal inertia of the heater located at the entrance to a duct for the time-dependent temperature field. The solution effectively addresses the instability of the thermal control system, influencing the design of a duct with a suitable thermal control system. Most importantly, RM's potential as a manufacturing process for polymeric components is limited by several concerns, including difficulties in the clarity of process control, long cycle time, narrow range of applicable polymers, and poor surface finish [10] . Results are limited to the experimental data, even if the fixed domain model consigns the most trustworthy data in the theoretical model and the semi-empirical approaches to the melting and crystallization state [11–17,27]. Researchers primarily assessed surface quality in terms of porosity prevalence [18,20,21], degradation severity [22], and warpage [22–24], given its significance in rotational moulding systems. Nonetheless, alternative sources claim that the acceleration of breakdown due to pressurising bubbles leads to the elimination of surface imperfections under pressurising moulding conditions [20,25,26].

The current analysis estimates that the Australian polyethylene market was worth $2.1 billion in 2018 and will reach $3.8 billion in 2024. Considering that Australia is the driest country in the world, it is crucial to store rainwater for harvesting purposes using sizable tanks and containers [28]. In 2022, the marketplace for water storage systems in Australia was projected to be valued at USD 152.08 million. BlueWeave [29] 2029 forecasts that the size of the Australian market for water storage systems will increase at a noteworthy CAGR of 8.49 % between 2023 and 2029, to reach a value of USD 282.59 million. This review paper addresses the anticipated future demand for rotationally moulded products by focusing on key challenges such as temperature variation, air leakage, pressure drop, and enhanced heat distribution techniques. The authors aim to provide valuable insights for the rotomoulding industry regarding improved heat transition within the oven, advantages of shape modifications in ducts, cost-effectiveness, and the benefits of utilising properly optimised insulated materials.

Table 1
Tabular representation of relevant research in the rotomoulding industry.

Key focus	Relevance	Source
Time-dependent heat transfer in a duct.	If the duct serves as a heat transport medium, process delay may be taken into consideration for this reason.	Gerardo et al. [9]
Examination of the rotomoulding process with available materials and product quality in future	Review paper on rotomoulding techniques which includes process and product quality.	Ogila et al. [10]
Accuracy in temperature prediction for inside mould and its surroundings.	Simulation-based observation of temperature changes in ducts.	Lim et al. [11–13] Greco et al. [15, 14], Bellehumeur et al. [15,16] Xu et al. [17,18, 16].;
Product quality development	Challenges in the mould-quality process related to temperature.	Spence et al. [18–20] Crawford et al. [21] Cramez et al. [22] Bawisker et al. [23] Pop et al. [24] Kontopoulou et al. [25]. Gogos et al. [26]

2. An insight into previous research conducted in the rotational moulding industry

2.1. Initial investigations into rotational moulding

Though being a distinctive process, the production cycle time of the rotational moulding machine is longer compared to blow moulding and thermoforming [30]. The slow characteristics in cycle time of the RM process can be highlighted as an alarming issue in mass production. The process completion time for a rotational moulding machine is between 40 −80 min [31]. Fig. 1 shows its process, which is based on four basic steps: (a) mould charging, (b) mould heating, (c) mould cooling, and (d) part ejection.

The rotational moulding machine process can be divided into six distinct phases [32].

Induction: Inserted powder form of the mould picks up the heat through the mould wall though it remains free until point 1.

Sintering: A sufficiently high temperature of the mould and the powder reaches while the successive layering of the powder attached to the inner surface starts. Absorption of energy during the melting of the polymer slows down the increase in temperature within the mould. There is a natural separation of particle size during sintering—smaller particles adhere first, followed progressively larger particles.

Consolidation: The heating continues to fuse and consolidate the material into a solid homogenous mass when the powder has adhered to the mould completely.

Melt-phase cooling: The molten polymer should be kept in moving condition to prevent wilting.

Crystallization: The energy will be released when the polymers will reach its crystallization temperature when the polymer is in cool condition. which maintains the internal temperature on a second plateau. This will not occur for amorphous materials.

Solid-phase cooling: Beyond the point at which the material has crystallized, the part is solidified and may pull away from the mould surface.

Regarding polyethylene moulds, several regular transition points are discernible. Phases are shown in the Fig. 2:

The process has been evacuated since stage 1, and a semi-plateau in the graph can be seen where the powdery bed is being depleted with ill-homogeneous melt containing numerous air bubbles. Point 2 depicts the densification period, which occurs when the peak internal air temperature (PIAT) is attained at point 3. Then, the pattern inverts, and cooling continues gradually until point 4. The end of crystallization and solidification occurs at point 5, when a semi-plateau is detected. A slight modification in the graph is noted at point (6), and the demolding

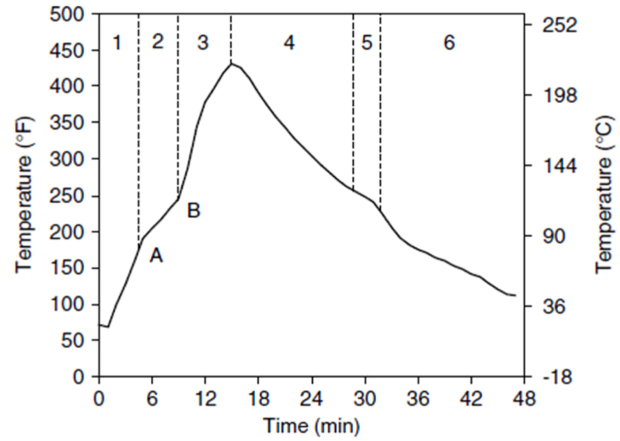

Fig. 2. Temperature during the six -phases of rotational moulding [32].

temperature is attained after this point [19] . Paul Nugget placed two thermocouples in the same process to measure and analyse the temperature profile in two different positions (shown in Fig. 3), one thermocouple was placed to measure the external environment of the mould, and the second one measured the internal temperature of the mould (the enclosed inner volume). Variation in the temperature of the roto-moulding cycle was observed due to the rapid movement of the air inside the oven and rotating mould passing the hot air inlet. After completion of the oven cycle, the environment temperature drops drastically to the cooling bay temperature. For enclosed coolers, heat radiating from the mould can raise the surrounding temperature initially, but this falls over a period as the mould cools [32].

Material fuses to the mould in waves as heating proceeds between points A and B. The rate at which the internal air temperature rises slows down and reaches a plateau because of the material absorbing energy during the melting process, which turns it from a powder to a solid molten mass. When all the material has attached to the mould surface at point B, the plateau ends, and energy is once again delivered directly to the inside air, causing the temperature to rise faster. Up to point C, there is still heating. The peak internal temperature recorded within may correlate with the final level of "cure" or "cook." The part's temperature decreases as the mould gradually begins to cool. The mould's exterior surface temperature increases faster than the mould's interior air temperature decreases (Fig. 4). This rate is mostly determined by the cooling technique (cooling through a fan before the cycle starts) and the external environment (summer cooling can be much slower than winter cooling). The mould continuously cools until crystallization occurs. This second

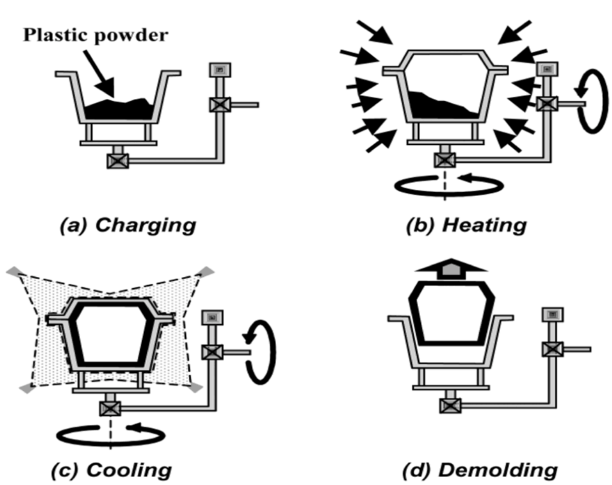

Fig. 1. Principle of rotational moulding, courtesy of The Queen's University, Belfast [31].

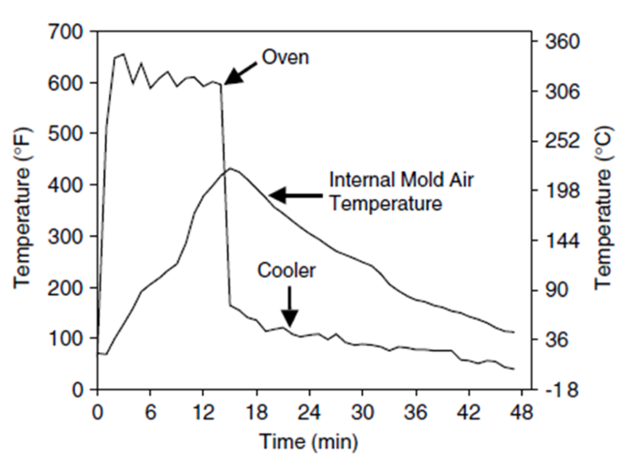

Fig. 3. External and internal temperature profiles during a typical moulding cycle for a polyethylene part [32].

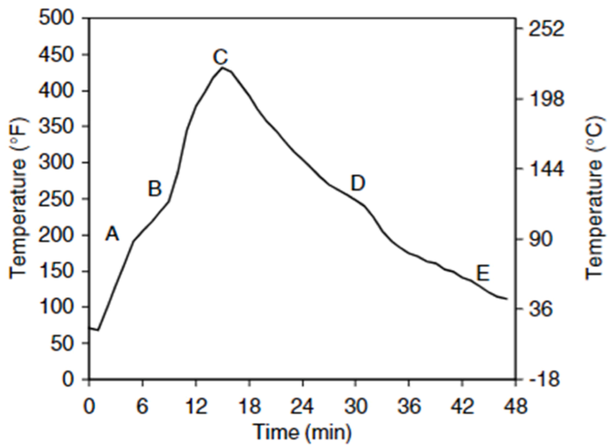

Fig. 4. Internal air temperature profile during the moulding cycle (polyethylene part) [32].

plateau, which resembles the melting plateau discovered during the cycle's heating stage, is created by energy generated during the formation of a crystalline structure, which keeps the part's temperature constant. This takes place at point D. Paul Nugget has tried to provide the phases of temperature variation in his book's chapter [19].

Hollow profiles and tubes are formed with centrifugal forces. Because of this, there must be a minimum revolution speed and a greater centrifugal force than the actual weight [34]. The gravitational acceleration (g) and the tube's radius (r) determine the minimum speed (n_{min}), according to Neitzel et al. [35].

$$n_{min} > \frac{1}{2\pi} \cdot \sqrt{\frac{g}{r}}$$

Current models put forth the assumption that polymer powders undergo constant turbulent stirring, maintaining a uniform powder temperature and allowing convection to control heat exchange at the interface [33,34]. Regardless, it is important to remember that, in this cycle, the amount of time spent using the powder is short concerning the overall processing time. Determining the core issue presents a significant challenge during the rotational moulding process, as the polymer powders experience multiple stages of transition, which include heating, melting, and solidification within biaxial rotational moulds. Nonetheless, both the endothermic and exothermic transitions have an impact on this heat transition process [38,35].

When rotational moulding or undergoing any other material phase transition operation, the latent heat of transition of the material is considered in the $\dot{q}$ term. As crystallization occurs, the $\dot{q}$ term takes on negative values, whereas during melting it takes on positive ones.

The total enthalpy is introduced.

$$h_T(\mathrm{T}) = c_p T + \frac{q}{\rho} \tag{1}$$

Once the problem has been defined through the enthalpy method (Eq. (1)), the different boundary conditions (BC) at the interface of regions characterized by different material properties need to be written. The BC at the external mould surface, in contact with the heating gases in the oven, has been assumed to be governed by convection [36,37].

$$k_p \frac{\partial T}{\partial z} = h_{mp}(T_i - T_m) \text{at } z = z_i \tag{2}$$

Here in Equation 2, Ti and Tm represent the temperature of the lower surface of the powder and the inner surface of the mould respectively, h_{mp} is the convection heat transfer coefficient at the mould polymer surface. z and z_i represents the dimension of spatial coordinates measured from the centre of the mould and coordinate of the mould's inner surface, respectively. The powder temperature history can be calculated through Fourier's Law of unsteady heat conduction in the following form (Eq. (3)) [38].

$$k_p \frac{1}{z^q} \frac{\partial}{\partial z}\left(z^q \frac{\partial T}{\partial Z}\right) = \rho_p c_p \frac{\partial T}{\partial t} \text{ for } z_t < z < z_i \tag{3}$$

The variables in this case are t, the time variable, z_t, the coordinate of the top surface of the powder layer and z_i is the coordinate of the inner surface of the mould. The density, specific heat, and thermal conductivity of the powder, respectively. Planar, axisymmetric, and spherical moulds are represented, respectively, by the values of q= 0, q= 1, and q= 2. Because of the product's size concerning its thickness, it is reasonable to exclude heat transmission in the circumferential direction for the spherical and cylindrical moulds.

The heat transfer from the plastic to the mould can be represented by Equation 2 with a single heat transfer coefficient at the mould-plastic interface. The representation of the equation from plastic to air mould can be expressed in the form –

$$\frac{1}{h_{mod}} = \frac{1}{h_{ma}} + \frac{1}{h_i} \tag{4}$$

Where, h_{mod} indicates, the heat transfer coefficient at the air gap, h_{ma} – heat flux at the mould–air and h_i – plastic–air interfaces. Thus, the effect of the plastic shrinkage on the overall heat transfer is reduced to estimating a suitable heat transfer coefficient at the mould–plastic interface [27].

Banerjee et al. [27] proposed a modified model where authors hypothesized the thermal transition at the mould-powder interface occurs due to convection and the heating of powder particles via conduction; however, the influence of endothermic and exothermic heat transition processes has not been addressed. It was later modified by A. Greco et al. [14] approaching a kinematic model where he solved a one-dimensional unsteady heat conduction equation using the finite difference method an increase in the product wall thickness due to the contact resistance between the powder and the mould affects the powder heating temperature and cycle time (Fig. 5).

2.2. Mould area enhancement and cycle time reduction

According to Khouri et al. [39], the mould to the cooling fluid, the polymer melts to internal air, and the oven to mould has the highest convective heat transfer coefficients. As per their research, the mould is essential for cutting down on process cycle times. They concluded that air amplifiers were the best option, with 25 % and 14 % reductions in the cooling time and the overall cycle time, respectively. To validate his finding M.Z Abdullah et al. [40] conducted both experimental and theoretical analysis on three types of mould ex: (a) Plain mould, (b) roughness-enhanced mould and (c) pin-enhanced mould and organized the CFD flow arrangement (Fig. 6) into three categories (a) Flow across, (b) Flow across at 45°,(c) flow normal to pin -enhanced mould.

It was observed from the experiment that the closer the tips of the pin the higher the air velocity. The representative value should be within the pin height and the steam passing between them.

From the leading edge to the trailing edge of the pin-enhanced plate, the average air speed data for each case were determined. The average airspeeds around pins produced by the CFD simulations as well as the average airspeeds according to the flow directions are shown in Table 1. Based on the spacing-to-thickness ratio, a chart representing average air speed was depicted using the identical data from Table 2 (refer to Fig. 7). The findings imply minimal gain by increasing pin spacing above an intrepid separation twice the pin thickness.

On the contrary, mould thickness plays a significant role in the cycle time reduction for the rotomoulding machine. The reduction of energy consumption during the heating process facilitates the use of thinner moulds, resulting in decreased cycle times and improved energy efficiency. Faster cycle time results in a higher productivity rate and helps

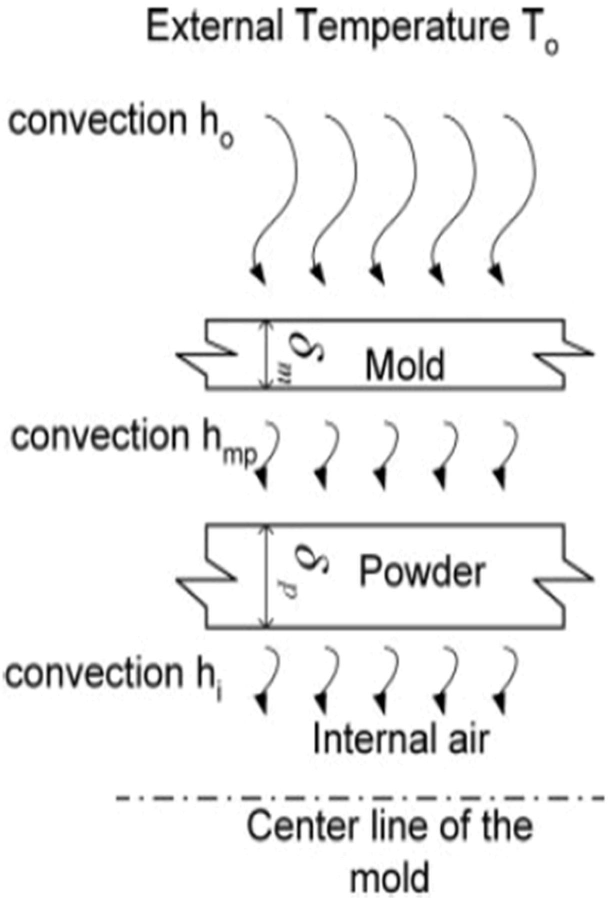

Fig. 5. Heat transfer from the oven to mould, powder and internal air [41].

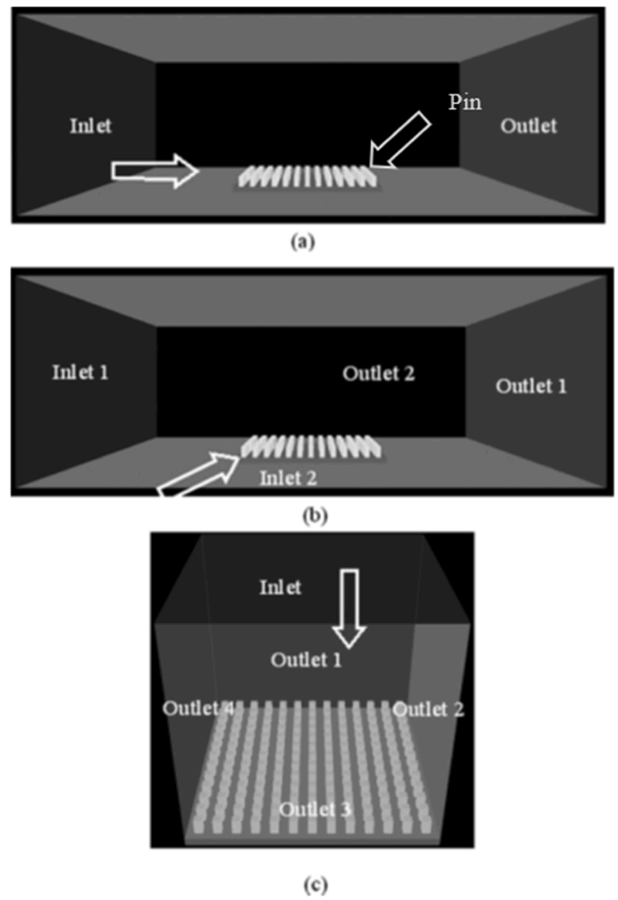

Fig. 6. CFD flow arrangement in Phoenix [40].

industries save production costs. By adjusting the measurements for the section wall thicknesses of 3.2, 6.0, 3.2, 6.0, and 9.0 (in mm), Abdullah et al. [41] aimed at validating the assumption. Two separate oven temperatures were used for the experiment:

a. defines oven temperature of 300 °C and
b. defines oven temperature of 380 °C, using two forms of improved mould roughness enhanced mould and pin-enhanced mould.

From Table 3, the experimental cycle time reduction was ~18 % and 28 % for the roughness-enhanced mould and pin-enhanced mould, respectively. On the other hand, predicted cycle time reductions were ~21 % and 32 %, respectively. The report indicates a link between the experimental and anticipated cycle times; more data on component wall thicknesses and part sizes would enhance the analysis.

The author demonstrated that cycle time reduction serves as a framework for mould enhancement in the rotational moulding process; however, their theoretical [40] and experimental [41] studies were confined to an aluminium cubic mould. The potential benefits alongside the drawbacks of mould upgrades for additional geometrically formed moulds remain unspecified.

3. Essential factors for production optimisation

3.1. Impact of duct size on air flow rate

If an RM machine industry is using a duct to flow the hot air through the duct to the oven, then there are some basic perspectives to highlight. In most cases, it is hard to maintain the same air velocity and temperature through the duct during the air-flowing condition. Thus, we tried to focus on the concepts of sustainable temperature and air distribution. Since, hot air flows through a duct and faces a variety of disputes ex: heat loss, air leakage, pressure drop, air quality, corrosion, thermal expansion, contraction etc.

Table 2
Average air speed values according to flow directions and the overall average air speed between the pins [40].

Flow direction & Speed	Spacing to thickness ratio				
	1.00	1.50	2.00	2.50	3.50
Flow across a plate; Average speed $\bar{u}$ (m/s)	5.8	7.5	9.7	10.2	10.5
Flow at 45° across a plate; Average speed $\bar{u}$ (m/s)	2.5	3.8	5.7	6.2	6.8
Flow normal to a plate; Average speed $\bar{u}$ (m/s)	4.7	5.2	5.8	5.9	6.2
Overall average speed; Average speed $\bar{u}$ (m/s)	4.3	5.5	7.1	7.4	7.8

In the context of air distribution, proper duct design is crucial because unplanned ducting design can result in resistance to inadequate airflow. If ducts are too large may lead to low velocity, stratification, and poor mixing on the other hand if the duct is too minuscule, resulting in pressure drop, noise, vibration and inadequate airflow (Fig. 8).

If the duct is completely sealed and no air leaks along the way, we can assume that, as per conservation law, every bit of the air that enters the duct on the left must come out of the duct from somewhere (Fig. 9).

Moreover, the Mach number of air is very small (lower than 0.3), hence considered an incompressible fluid [42]. However, there can be a change in density if there is a considerable temperature change. The equation becomes simpler for incompressible flow, which is frequently a realistic assumption for air at moderate speeds.

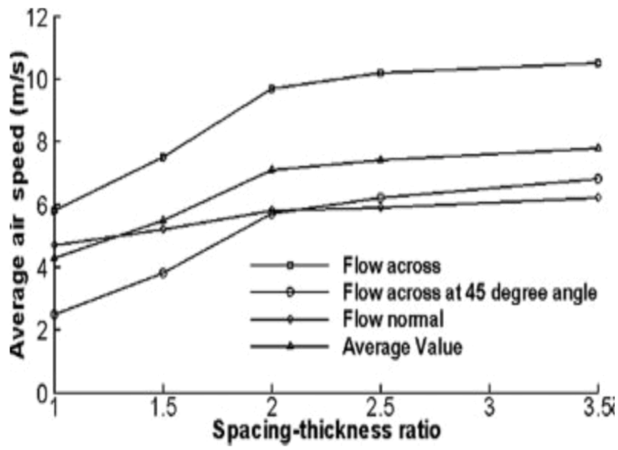

Fig. 7. The average air speed according to the flow directions and the overall average air speed between pins [40].

Table 3
Summary of the comparison between experimental and predicted cycle time [41].

Mould type	% Cycle time reduction				
	3.2[a]	6.0[a]	3.2[b]	6.0[b]	9.0[b]
Roughness-enhanced mould (experimental)	17	19	16	20	16
Pin enhanced mould (experimental)	32	28	26	25	28
Roughness-enhanced mould (prediction)	21	21	21	21	20
Pin enhanced mould (prediction)	32	32	32	32	31

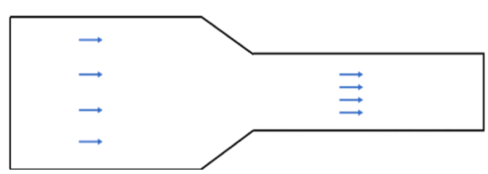

Fig. 8. A large size duct along with a reducer and a smaller duct.

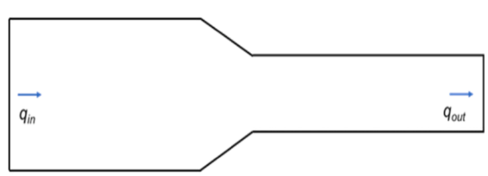

Fig. 9. The airflow rate entering the duct is the same as the air leaving the duct.

$$A_{in}\upsilon_{in} = A_{out}\upsilon_{out}$$

The cross-sectional areas of the duct at the inlet and outlet are denoted as A_{in} and A_{out}, respectively. The air velocities at the intake and outlet are denoted by υ_{in} and υ_{out}, respectively.

Moreover, the conservation of energy is important in the ducting system for maintaining efficiency, ensuring proper operation, predicting flow behaviour, designing efficient systems and optimizing performance. But, in the case of high-temperature air flow, there can be a change in temperature and pressure. Due to fluctuations in temperatures, there will be a change in density.

The kinetic theory of gases and ideal gas law plays the role of basic principle in this situation.

Bernoulli's equation describes the conservation of energy in a flowing fluid and can be applied to air in the duct. This equitation is used at the time of change in temperature and pressure in a small duct. Assuming steady, incompressible flow and negligible viscosity, Bernoulli's equation is

$$P + \frac{1}{2}\rho\upsilon^2 + \rho gh = constant \tag{5}$$

For horizontal ducts, ρgh can be ignored as $\Delta h = 0$. Thus, $P + \frac{1}{2}\rho\upsilon^2 = constant$ (6)

Here, P, ρ, υ, g, h denotes pressure, air density, air velocity, gravity due to acceleration, and height above a reference level, respectively. Furthermore, changes in the duct cross-sectional area refer to changes in the velocity and the pressure of the incompressible fluid. Gao et al. [43] have focused on the aspect ratio and curvature radius of the bend. In the study, scholars expressed the aspect ratio by D_1/D_2, the curvature ratio as R/D_0 . Moreover, the authors explored the aspect ratio and the radius of curvature on the drag and core speed in "U" and "S" shaped ducts. This study utilised the widely recognised CFD software Fluent for analysis, while pre-processing was executed using ICEM–CFD. Numerical simulation can give better outcomes in subtle changes in the fluid flow rate and dragging of the duct system than experiments [44,45]. Moreover, duct diameter has prime importance in reaching adequate airflow to the face [46].

In Fig. 10, the S-shaped bend has a lower inertia force of the downstream fluid than the U-shaped curve as it mainly depends on pressure gradient force. As a result, R/D (ratio of the radius of the centre arc and bend diameter) has a minimal impact on the force of inertia. Increased R/D does not significantly reduce the inertial force of the S-shaped bend, resulting in a slight drop in core speed. It represents the authenticity of the continuity equation in an incompressible fluid. The cross-sectional area in the geometry of a duct changes due to the bend, therefore the area may decrease. Hence, the velocity increases in the local resistance areas to maintain a constant mass flow rate.

3.2. Geometrical model analysis of ducts

Proper design of ducting is essential for air flow due to several reasons, encompassing efficiency, high performance, and cost reduction. Generally, a proper ducting system helps in heat loss and gain (properly insulated and sealed), air distribution, and pressure balancing. In order to ensure that hot air is distributed correctly through the duct, this review paper will focus on a few ducting models.

The fabric air dispersion system (FADS) has been introduced due to the limitation of the air conditioning system. FADS is made of a special type of polyester fibre and comprises a set of air distribution and supply ducts. Moreover, it offers numerous advantages such as a uniform air supply, easy installation, no blowing sensation, quiet operation, lightweight design, and simple cleaning and disinfection. However, it also has some drawbacks like air leakage due to seams and joints, pressure drop due to friction, duct length and configuration, and poor air distribution efficiency due to design and perforation. FADS has gained significant attention in various sectors such as shopping malls, factories, stadiums, and theatres [47]. The number of rows, hole spacing and other parameters that result in various opening configurations can be varied due to duct opening [48].

In scenarios where the number of openings remains constant, an increase in the number of rows leads to a more rapid decay of wind speed within the tube. The number of open rows in the FADS is negatively correlated with the flow velocity in the tube, and higher numbers of rows result in lower flow velocity and greater temperature rises. Therefore, FADS with more rows of openings exhibit a higher temperature rise and higher temperatures at the same location inside the perforated tube (Fig. 11).

The three FADS, depicted in Fig. 12, were incorporated to demonstrate that elbows, acting as airflow obstructions, result in variations in

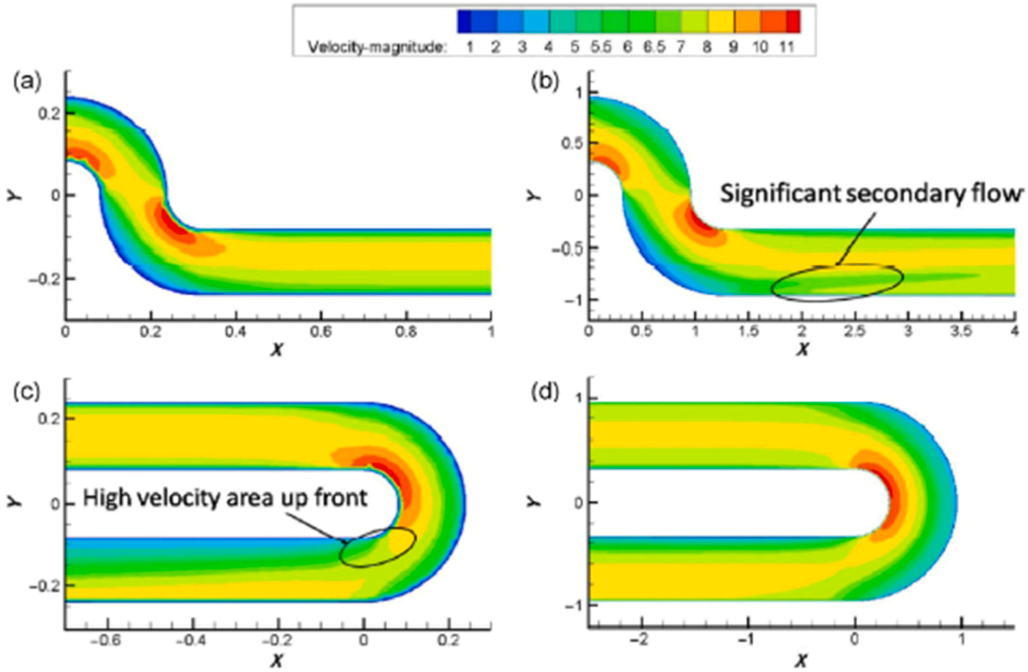

Fig. 10. Vertical section for the bend flow field: (a) with the S-shaped connection, $D1/D2$ = 5:1; (b) with the S-shaped connection, $D1/D2$ = 1:5; (c) with the U-shaped connection, $D1/D2$ = 5:1; and (d) with the U-shaped connection, $D1/D2$ = 1:5 [43] .

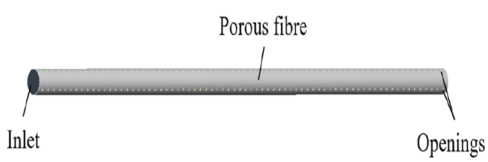

Fig. 11. Schematic diagram of an ejection permeable FADS [49].

air velocity. In this scenario, the a)"1″ shape is considered a uniform medium, whereas the b)"L" and c)"U" shapes of FADS are viewed as mediums containing one and two elbows, respectively, as obstacles. This form illustrates the decrease in airflow caused by obstacles and specific alterations in central areas.

3.2.1. *Air-flow field characteristics*

In Fig. 13, the “1 “-shaped FADS shows the slowest decrease in speed, followed by the “L” – shaped FADS. Whereas the “U “-shaped FADS shows the fastest decrease in speed.

Table 4 summarizes the vital details regarding the velocity profiles for various FADS (Flow Acceleration Device System) forms as a function of distance from the inlet position.

The results underscore the significant impact of both FADS configuration and elbows geometry on fluid velocity. The "I"-shaped FADS is the most efficient design for sustaining high velocities, succeeded by the "L"-shaped FADS, whilst the "U"-shaped FADS demonstrates the least effectiveness. The findings indicate that optimising FADS design and reducing the quantity or sharpness of bends in the pipeline may be essential for improving fluid flow efficiency in practical applications.

3.2.2. *CFD field characteristics*

In Fig. 17, temperature variation is evident due to the local resistance aka elbows’ sudden temperature rise and sudden drop of temperature being seen especially in “L”-shaped (Fig. 15) and “U” -shaped (Fig. 16)

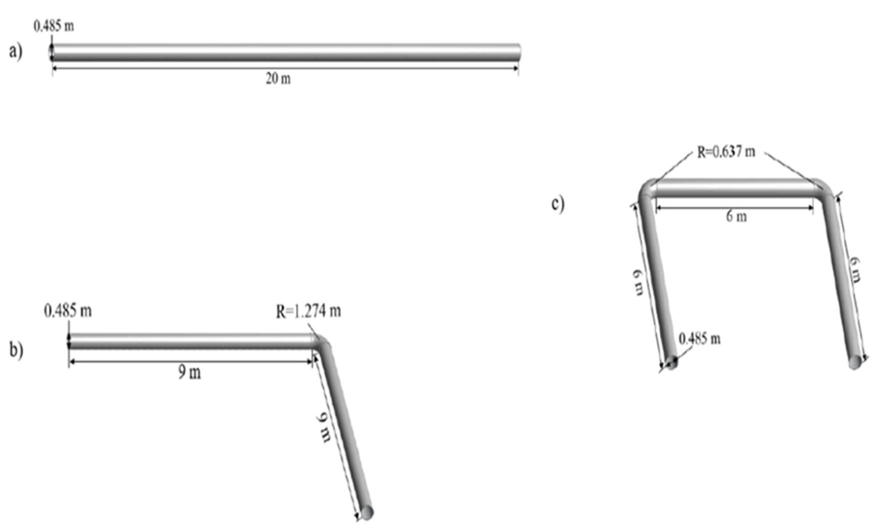

Fig. 12. Different FADS shapes, a) “1″ shape, b) “L” shape & c) “U” shape [49].

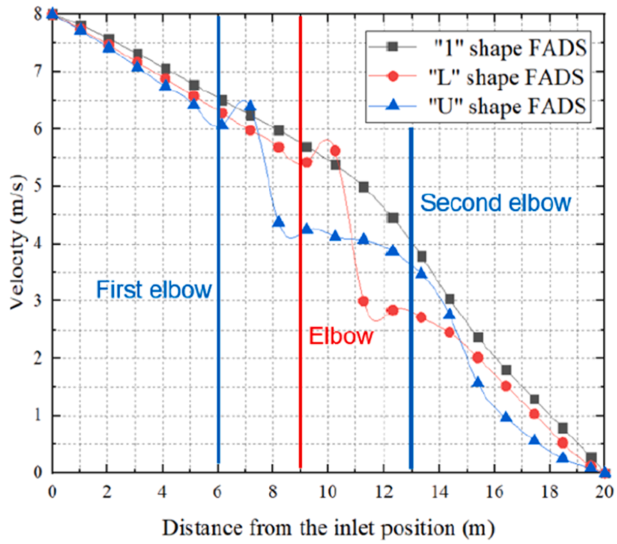

Fig. 13. Internal velocities for three different shapes of FADS [49].

Table 4
Velocity profiles of multiple FADS configurations along the pipeline.

Distance from Inlet (m)	I-shape FADS Velocity (m/s)	L-shape FADS Velocity (m/s)	U-shape FADS Velocity (m/s)
0	8	8	8
4	~7.5	~7.2	~6.8
8	~6.5	~6.0	~5.0
10	~5.5	~4.5	~3.5
12	~4.5	~3.5	~2.5
14	~3.5	~2.5	~1.5
16	~2.5	~1.5	~0.8
18	~1.5	~0.8	~0.5
20	~0.8	~0.5	~0.2

FADS, whereas the “1″ shape (Fig. 14) FADS, shows smooth temperature distribution and temperature rise with low turbulence than “L”- shaped and “U”-shaped FADS. Yang et al. [52] applied the FLUENT porous media model for simulation by establishing boundary conditions at four locations: the front end, rear end, openings, and pressure outlets. Boundary types include velocity inlet, wall, and pressure outlet, with specified conditions of 8 m/s, 20 °C, and 0 Pa, respectively.

The positions marked in circles show the temperature distribution in the shapes due to geometrical changes. There are noticeable changes in the temperature profile at each elbow corner and a decrease in air velocity due to local resistance inside the tubes. The significance of geometrical changes in the duct is being analysed with the aid of the examples. The saturated temperature is visible from a substantial distance in a uniform profile ("1″ shape FADS). In "U" shaped FADS, the temperature profile rapidly alters following each elbow corner due to local obstructions.

The authors found that, while air velocity affects the temperature rise inside the duct, a higher number of rows opening causes the air velocity to decay and raises the temperature. Due to the disruption of the duct’s airflow caused by the elbows used as resistance in the midpoints, there is increased turbulence and primarily non-uniform air distribution. Straight ducts and minimal elbow engagements were the author’s

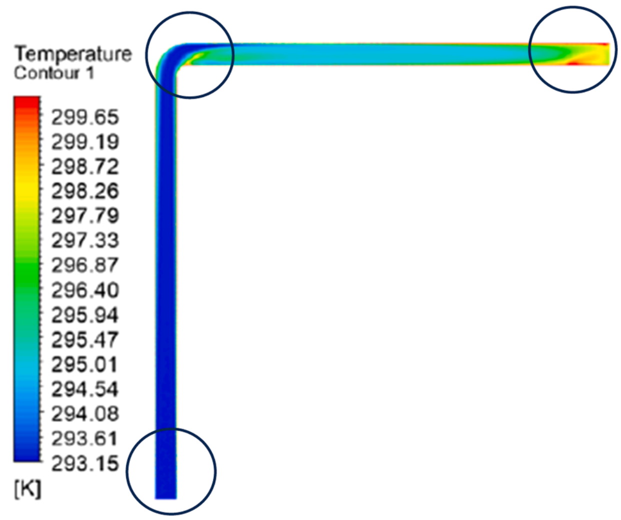

Fig. 15. “L”-shaped FADS temperature distribution [49].

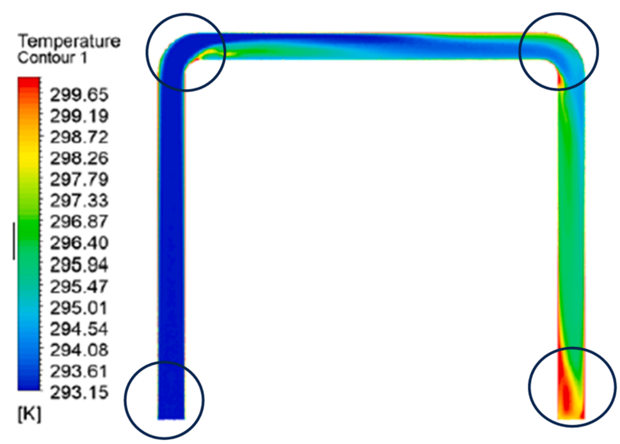

Fig. 16. “U”-shaped FADS temperature distribution [49].

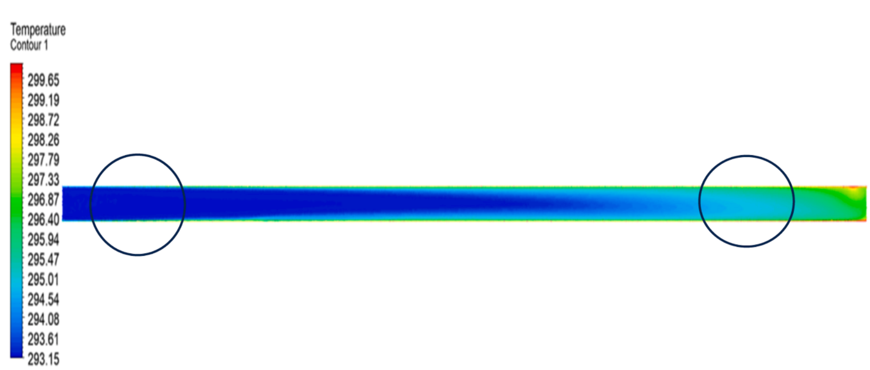

Fig. 14. “1″-shaped FADS temperature distribution [49].

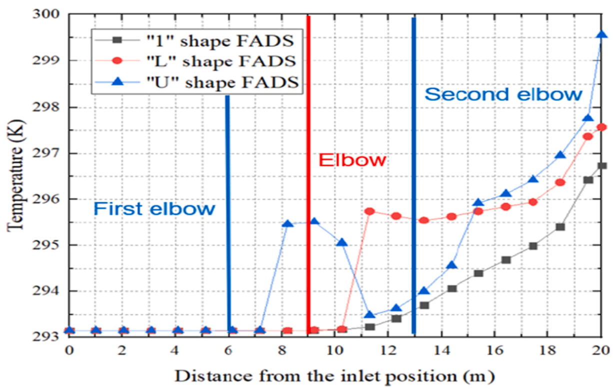

Fig. 17. Temperature variation along internal resistance of three different shaped FADS [49].

recommendations. Despite developing a fresh idea that begs for additional research, the author failed to place an emphasis on accuracy at the industrial level. Furthermore, Hekal et al. [50], tried to bridge between experimental and CFD simulation assessment. Therefore, conducted laboratory and numerical experiments to determine a specific calculation technique for the friction factor and Nusselt number within fabric air ducts. Additionally, developed a validated CFD air distribution model that can predict airflow patterns and heat transfer parameters across various configurations of fabric air ducts. The findings indicated that the maximum discrepancy between laboratory and numerical values for the mean friction factor and mean Nusselt number was 4.9 % and 4.8 %, respectively.

To validate the hypothesis, the authors performed both CFD simulations and experimental tests on the same duct. The CFD simulation was conducted using ANSYS R19.1 software.

Table 5 presents the relative percentage error between the mean Nusselt number and the mean friction factor for both experimental and simulated results. The relative percentage inaccuracy in the mean Nusselt number ranges from −2.9 % to 4.8 %, whereas the friction factor varies from 1.6 % to 4.9 %.

Manufacturing companies that produce Fabric Air Ducts (FADs) usually offer comprehensive catalogues that depict essential connections between important performance parameters, including pressure drop in relation to discharge, friction factor in relation to discharge, and velocity in relation to pressure drop. These relationships are crucial for engineers and designers to assess the performance of FAD systems across different operating conditions. Nonetheless, although these catalogues differ among manufacturers regarding design specifications and material properties, the primary objective remains the same; that is, determining a system that reduces both initial and operating costs, thus enhancing energy efficiency.

4. Considerable design parameters and the importance of ribs as a structure

4.1. Pressure drops and near-wall treatment inside the duct

Designing ducts plays an important role in influencing pressure drop (ΔP), along with duct geometry (Length, diameter and surface roughness) of the duct. A region of recirculation of flow and turbulence is created due to the airflow separation. Hence, it causes additional friction and energy dissipation. The elbow bends present challenges in accurately measuring and representing pressure loss. Cai et al. [51] established an empirical correlation for predicting pressure loss in 90° elbow bends; however, Kunabeva et al. [52] recommend utilising divergence to alter airflow direction instead of employing a severe 90° bend.

Later, Walunj et al. [53] made an analysis based on ducts having two different types of bends (a) 90° sharp bands and (b) Y-section bends. The authors concentrate on the utilisation of computational fluid dynamics (CFD) simulation tools to investigate the velocity distribution of air in the duct at various sections, the pressure difference at various outlets, and the distribution of airflow and conclude stating, that the gradual bend instead of sharp bends for branching in the ducting system reduces the pressure loss.

The graph in Fig. 18 shows, the pressure drops across the duct having Y- shaped bend has less pressure drop than the duct with a sharp 90 ° bend. Other than duct bend, slop angles (β) have some vital importance in reducing the pressure loss as well as the impact on Nusselt (*Nu*) and Reynolds (*Re*) numbers. Zhang et al. [57] have taken the reference data from Junqi et al. [59] to substantiate the assertion that the pressure loss in trapezoidal and rectangular ducts escalates with an increase in the Reynolds number. TPF (Thermal performance factor) is being introduced to consider the influence of convective heat transfer performance and pressure drop ΔP and assess heat transfer enhancement degree [60].

$$TPF = \frac{Nu_j}{Nu_y} \Big/ \left(\frac{f_j}{f_y}\right)^{1/3} \tag{7}$$

Here, Nu = Nusselt number, f = flow resistance co-efficient, j =different slope angles & y =rectangular duct having 0 ° slope angle.

The author noted that as the slope angle increases, the Nu number also rises in conjunction with a pressure drop in rectangular and

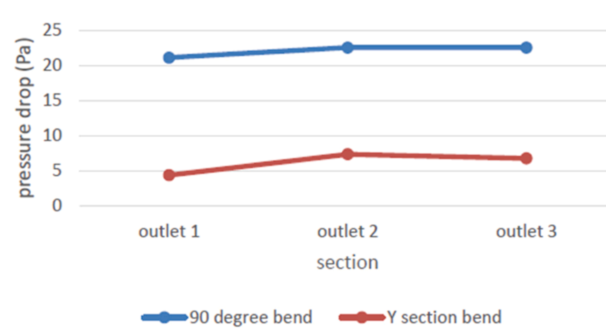

Fig. 18. Graph showing pressure drop across the duct [53].

Table 5
Validation chart of the percentage error between experimental and CFD result of Hekal et al. [50].

Mean Inlet velocity (m/s)	Mean inlet temperature (°C)	Mean Inlet Pressure (Pa)	Fan Speed (RPM)	f_{Exp}	f_{CFD}	% Error in f	Nu_{EXP}	Nu_{CFD}	% Error in Nu
1.88	40.5	57.77	822.5	0.167	0.165	1.6	161.46	153.73	4.8
1.47	42.5	38.7	705	0.185	0.184	0.6	160.33	160.33	0
1.39	44.94	31.77	587.5	0.202	0.193	4.6	160.24	152.43	4.9
1.31	47.49	19.5	470	0.217	0.213	1.7	160.11	161.4	−0.8
0.55	48.29	11.18	352.5	0.238	0.227	4.8	159.29	163.86	−2.9
0.49	68.55	5.75	235	0.249	0.243	2.5	140.22	139.06	0.8

trapezoidal ducts. Wang et al. [54] have performed numerical simulations in regular polygonal ducts (Fig. 19) to identify the turbulent flow and heat transfer coefficient. They proposed a correction factor to predict the turbulent heat transfer in regular polygonal ducts through these simulations.

Wang et al. [54] showcased high *Re* number indicates more turbulence inside the duct. Furthermore, the discrepancy between the average Nusselt values for the circular tube and regular polygonal ducts rises as the regular polygon's number of sides decreases. In other words, using hydraulic diameter for noncircular ducts—like the equilateral triangular duct—will lead to unacceptably high inaccuracies, roughly 27.5 %. Furthermore, Zang et al. [55] noted enhanced and efficient uniform heat distribution in parabolic ducts, which optimises heat transfer performance by 5.1 % compared to trapezoidal ducts and by 25.4 % compared to rectangular ducts. Meanwhile, Chandratilleke et al. [56] investigated the airflow through a heated horizontal rectangular duct where they considered the natural convection (Gr<1000,000) heat transfer and thermal radiation from the duct wall. Traditionally, thermal radiation has been linked to high temperatures. However, new research indicates that thermal radiation can also contribute to mixed-mode heat transfer at moderate surface temperatures. It may additionally enhance natural convection, which in turn increases overall heat dissipation rates in heated ducts [57–60] . Nu fluctuations are supposed to be created due to the wall surface radiation, which refers to the thermal instability of the flow. Furthermore, Maximilian et al. [61] sought to highlight the heat transfer and fluid flow contrast in the stator duct utilising two distinct turbulence models (a) Stage model & (b) Frozen Rotor model; in addition to various near-wall treatments using CFD (ANSYS CFX). As per Boglietti et al. [62] and Kral et al. [63] simulation time in CFD depends on the number of elements used in it. Additionally, the analysis of turbulence within the duct is enhanced by the application of SST (Shear Stress and Transport), yielding more accurate results. Sørensenet al. [64] said the SST model concludes the RANS (Reynold-averaged Navier -Strokes) equation system by defining two more equations. As stated in Ansys CFX [65], the SST model combines the advantage of *k-ω* and validity at the distance flow field with the privilege of k-*ε* model. Furthermore, Menter et al. [66] highlighted the accuracy of the SST model for precise calculation of heat transfer coefficients. Chaube et al. [67] used ANSYS FLUENT for a duct with 10 different ribs and concluded by stating that the SST *k-ω* model came up with good results prediction. In contrast, the transitional flow exhibited a minor rise in heat transmission, while the fully rough flow showed a significant increase in friction. Apart from this automatic near-wall treatment is used in simulation to define a function which switches automatically from a low Reynolds number to a wall function treatment [65,68].

The logarithmic wall treatment must contain the first cell adjacent to the surface [61].

$$u_T^{vis} = \frac{u}{y^+} \tag{8}$$

Eq. (8) illustrates the velocity profile within the viscous sublayer, the area adjacent to a solid surface where viscous forces prevail over turbulent forces.

$$u_T^{log} = \frac{u}{\frac{1}{k}ln(y^+) + C} \tag{9}$$

Eq. (9), depicts the velocity distribution in the logarithmic area, situated beyond the viscous sublayer although still within the boundary layer.

$$u_T = \left[\left(u_T^{vis}\right)^4 + \left(u_T^{log}\right)^4 \right]^{0.25} \tag{10}$$

Eqs. (10) and (11) integrate the velocity scales from the viscous sublayer and the logarithmic region into a unified expression.

It is crucial to locate the initial cell adjacent to the surface in the logarithmic wall treatment and the scalable wall treatment using merely the logarithmic wall function is used in the $k-\varepsilon$ turbulence model.

$$\frac{u}{u_T} = \frac{1}{k} ln(\tilde{y}^+) + B \tag{11}$$

$\tilde{y}^+ = max\ (y^+, y^+_{lim}$ For y^+_{lim}= 11.06; where, $y^+_{max} = y^+ \le 11.06$ [69]

The $k-\varepsilon$ turbulence model parameters remain unchanged when compared to the SST turbulence model solution. Using the SST turbulence model, the computed value of the heat transfer coefficient changes when the mesh is refined. When the linear and logarithmic wall treatments cross and the largest error deviation is found, the maximum peak is around$y^+ \le 11.06$ [70]. Computational fluid dynamics (CFD) makes extensive use of the Shear Stress Transport (SST) k-ω turbulence model due to its precision in describing near-wall flow behaviour, particularly when dealing with negative pressure gradients and boundary layer separation. Ensuring adequate wall treatment is an essential component of adopting the SST k-ω model. This entails keeping a precise $y+$ value near 1 ($1 \le y+ < 5$). Particularly for flows characterised ($y+ > 5$) by large pressure gradients or separation, this can result in diminished precision. In an experiment, Georgi et al. [71] noted that the cell centre situated within the range of $5 < y+ < 11$ produces the most significant inaccuracy, even when employing the appropriate boundary condition.

An investigation was conducted by multiple scholars focusing on the enhanced performance of heat exchangers through the utilisation of different turbulators, including ribs, baffles, delta winglets, vortex generators, rings, and perforated blocks/baffles. This approach leads to improved heat transfer and a reduction in pressure drop. High heat resistance is primarily caused by the presence of a laminar sub-layer between the absorber plate and the moving air. The two repeating ribs' artificial geometry causes flow separation and reattachment, which causes turbulence in the laminar sublayer along with heat transfer enhancement. By implementing perforated ribs, to lower pressure drop, the roughness element's height could be kept low [72].

Gee et al. [72] analyzed the friction factor and heat transfer in three different (30°,49°,70°) angled helical-rib surfaces and concluded that the 49° helix angle rib provides the best performance. According to Thianpong et al. [73]. twisted rings give lower Nu and *f*, except at the

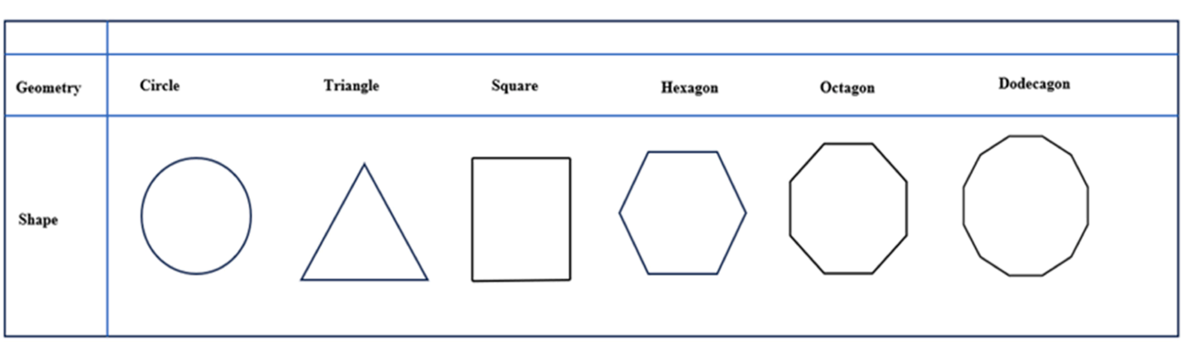

Fig. 19. Regular polygonal ducts [54].

largest width ratio ($W/D = 0.15$) and pitch ratio ($p/D = 1.0$) than common circular rings (CRs).

Apart from these, authors found maximum thermal performance congruous with smaller width and pitch ratio values. Tabish et al. [74] in their review highlighted that perforated bafflers are thermos-hydraulically better than solid bafflers. The authors recommended that the perforated delta compound winglets can better minimize pressure drop than the vortex generator. Webb et al. [75] investigated the enhancement of heat transfer techniques and the development of correlations for various fin configurations. Their findings indicate that the use of inserts and ribs improves the heat transfer rate, albeit with a corresponding increase in low-pressure drop. Ranjan et al. [76] assessed the hydrothermal performance associated with the combined application of five distinct enhancement techniques. (1) transverse ribs featuring a twisted tape insert with oblique teeth, (2) an integral transverse corrugation combined with a centre-cleared twisted-tape insert, (3) a transverse rib paired with a helical screw-tape insert, (4) axial ribs alongside a centre-cleared twisted-tape insert, and (5) an integral transverse rib with a centre-cleared twisted-tape insert. Performance evaluation indicates that the combination outperformed all individual inserts. Moreover, with the combination techniques, industries can achieve a **31–52 %** increase in heat duty at constant pumping power and in the point of energy saving, these techniques reduce **25–36 %** pumping power at constant heat duty.

5. Economic viability in the global market

The cost associated with the rotational moulding method mostly depends on energy sources and subsequently on the process itself. A cost-effectiveness comparison is conducted for a water tank manufacturer utilising a gas-fired oven. The oven's burners are isolated by a chamber (e.g., duct) and a circular fan to provide uniform temperature distribution throughout the oven. In this case, natural gas has been designated as the energy source for the calculation. An estimated analytical comparison of the manufacturing improvement based on six major parameters with assumed data is highlighted in Table 6.

If compared to heating a large area without any restricted air movement, using a duct system to distribute heat across a space eliminates heat loss and allows for more effective heating. As a result, less fuel is needed to attain the same temperature.

Adjusted annual fuel consumption = Annual fuel consumption /Thermal efficiency

Cost *per* Cycle in AUD =Fuel Consumption *per* Cycle × Cost *per* m^3(12)

Annual energy cost = Adjusted annual fuel consumption × Cost of natural gas (13)

Table 6
Comparison of oven efficiency, fuel consumption, and costs with and without ducting.

Parameter	Without Ducting	With Ducting
Energy source	Natural gas	Natural gas
Thermal Efficiency (%)	70 %*	85 %*
Fuel consumption per cycle (m^3)	10**	8.5**
Adjusted annual fuel consumption (m^3/year)	85,714.28***	70,588***
Initial Investment (AUD)	20,000	20,000
Annualized ducting cost (10-year time span)	N/A	2000
Cost of Natural Gas (AUD per m^3)	0.47	0.47
Number of Cycles per Day	20	20
Working days per year	300	300

* Thermal efficiency (η)=(Heat transfer to the Mold /Total heat Input) × 100
Assumptions: Total heat input /cycle =100,000 Kcal
Heat transfer to Mold (without duct) =70,000 Kcal, therefore,**70 %** efficiency.
Heat transfer to Mold (with duct) =85,000 Kcal; Therefore,**85**% efficiency.

Total annual cost (AUD) = Annual energy cost + Annualized ducting cost (14)

Referring to equation 12, the Fig. 20 graph shows that a roto-moulding machine without a duct costs 4.7 AUD per cycle at 70 % efficiency and 3.99 AUD per cycle at 85 % efficiency. The potential for future savings is suggested by the decreasing trend in the per-cycle cost. The annual cost in AUD, as illustrated in Fig. 21, is calculated by referring to equation 14, this leads to annual savings of 4260 AUD by employing a ducting system, where the annual energy costs are 40,286 AUD/year without ducting and 33,176 AUD/year with ducting, as indicated by equation 13. The annual ducting expense will be included in the annual cost of the oven that operates via the ducting system.

Rotational moulding industries that implement a ducting system in the oven can expect annual savings of 5110 AUD/year, reflecting approximately **12.7 %** in cost reductions each year. Furthermore, with an extra investment of 5000 AUD, the payback period will be approximately ∼ 1 year.

6. Proposed methods for better quality production

6.1. Selecting insulation material for better results

In the industry, the emphasis is consistently placed on minimising production costs while maximising efficiency and reducing energy consumption. Insulation systems can play a vital role in the field for effective heat transfer rates with low energy consumption. The rotational moulding machine needs convective heat flow through the duct where insulations minimize the heat loss from the duct surface to the surrounding ambient air. Moreover, a constant internal temperature can be gained by dint of the insulation. Utilising materials with low thermal conductivity is recommended to reduce heat loss and enhance energy efficiency. Ceramic fibre insulation, calcium silicate insulation, mineral wool insulation, high-temperature blanket insulation and refractory insulation are recommended to insulate the heat source of the rotational moulding machine. The thickness of the insulation plays a vital role since the thickness of the insulation increases, the more heat loss decreases [77,78]. Material selection for insulation, considering thermal factors, is crucial (Table 7).

According to Wong et al. [84], critical heat transfer occurs when the outer radius of the insulated circular duct is less than its critical insulation radius for small-sized ducts, especially in conditions of low ambient air/gas convective coefficient (h_0) . The thermal conductivity of insulation materials is influenced by variations in moisture content and temperature. Additionally, condensation within the insulation develops when the concentration of water vapour attains saturation levels [85].

6.2. Insulation thickness in duct reducing carbon emission

Bahadori et al. [86] proposed a method which inclines in excellent agreement with the reported data for a wide range of conditions where the average absolute deviation is calculated between the reported data and the proposed method which is ∼ 3.25 % correlating to the thermal thickness. Moreover, the author claimed the acceptance of the simplification of the method to any industrial application.

There is a correlation between insulation thickness and carbon emission. The reduction in carbon emission due to Optimum insulation thickness (OIT) varies for the different heat sources (NG, bagasse, coal, LPG, RH) between 11.23 −34.04 kg/m-year for NG. Moreover, Fig. 22 shows that it varies from 81.81 −318.33 kg/m-year for bagasse,40.73–123.43 kg/m-year for coal, 14.57–50.14 kg/m-year for LPG,20.38–56.39 kg/m-year and 37.04–141.59 kg/m-year for RH. Not only, CO_2 but also CO and SO_2 varies between the range of emission between 53.64–81.8 %,53.62–81.76 % and 49.64–76.66 % respectively for different parts and energy sources [87]

Insulation thickness is pivotal in ascertaining the energy efficiency of

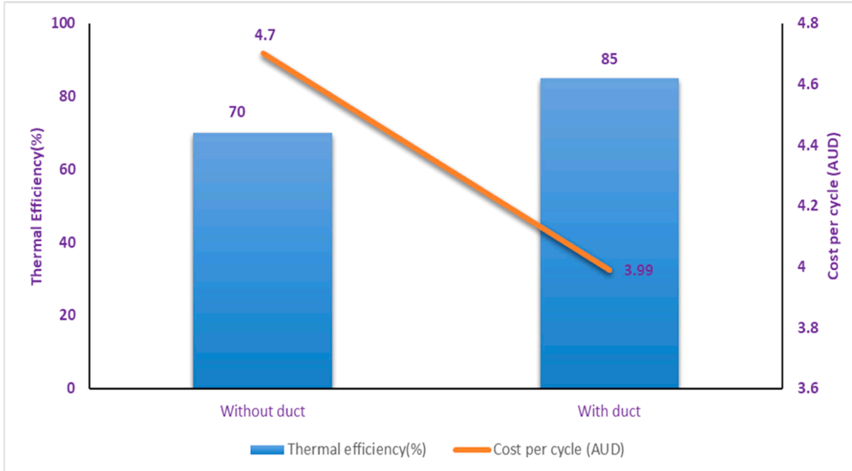

Fig. 20. Thermal efficiency vs Cost per cycle (AUD) graph for the rotomoulding industry.

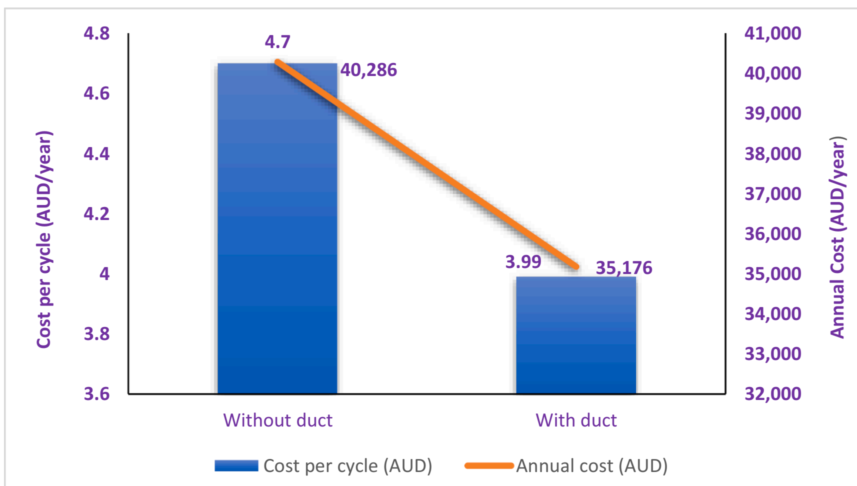

Fig. 21. Cost per cycle (AUD) vs Annual Cost (AUD) graph for the rotomoulding industry.

Table 7
Different thermal insulation for the heat source with high-temperature resistance.

Sl.	Author	Insulated fibre material	Density (kg/ m^3)	Thermal Conductivity (W/Mk)	Specific heat capacity (J/kg.K)	Temperature range °C	Remarks
1	Avikal et al. [79]	Calcium Silicate (Ca_2O_4Si)	250	0.014	1030	-	-
2		Rock mineral wool	144	0.044	840	-	-
3		Cellulose	65	0.04	2020	-	-
4		Phenolic foam	35	0.02	1000	-	-
5		Polyurethane	35	0.023	1450	-	-
6		Aerogel	1.5	0.014	1000	-	-
7	Mittenbuhler et al.	Kao wool ($Al_2O_3 - SiO_2$)	–	–	–	450°-800°	–
8	[80]	SiO_2(Pure)	–	–	–	700° –900°	–
9	Alkan et al. [81]	Bonded Fibre Ceramic	320	0.25	-	**max** = 1200°	Elastic behaviour, isotropic fibre distribution
10	Mineral Wool	-	0.04	–	- -		–
11	Levinson et al. [82]	Fibreglass (Flexible branch duct)	13	0.047	-	-	–
12		Fibreglass (Rigid duct)	24	0.018	-	-	No temperature range mentioned
13	Barkhad et al. [83]	Polylactic Acid (PLA)	-	0.0682	–	–	–

structures, industrial systems, and transportation. Insulation minimises energy consumption for heating and cooling by limiting heat transfer, hence directly affecting carbon emissions. Li et al. [88] observed the optimal thickness of glass wool insulation ranges from 0.010 m to 0.275 m; beyond this optimal thickness would have adverse effects. Disregarding future fluctuations may result in an overestimation of the insulation installation's capacity to reduce whole-life energy consumption and, consequently, emissions.

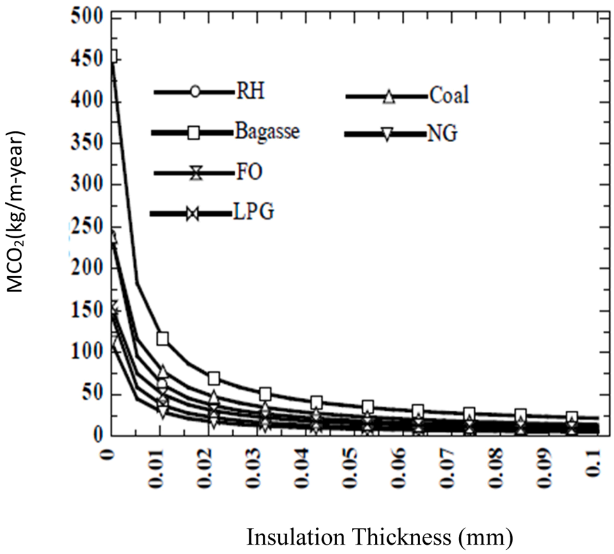

Fig. 22. Insulation thickness vs. CO_2 emission [87].

In Fig. 23, the graph refers to the optimal insulating thickness ranges from 0.050 m to 0.150 m, with total life energy consumption reduction between 27.165 and 39.321 kWh/m^2, while total whole life carbon emission reduction rises from 0.335 to 2.562 kgCO_2e/m^2.

Apart from the energy consumption reduction and carbon emission adding insulation in an oven for the rotomoulding process will direct profit for manufacturing companies in the sense of net savings over the system's lifespan.

Whole-of-life cost = Capital Expenditure + Total Maintenance Costs + Total Operating Costs + Other Costs + Disposal Costs – Residual Value (15)

[89]

In a scenario where a rotational moulding facility implements an upgrade to its oven insulation over a period of five years, the initial investment is projected at 50,000 AUD. The total operating cost is estimated at 5000 AUD per year, while the annual maintenance cost is calculated to be 3000 AUD. Additional expenses, including disposal costs, amount to 2000 AUD. Assuming an annual energy saving of 20,000 AUD, as indicated in equation 15, the total net savings over a period of 5 years will amount to 35,000 AUD.

7. Conclusion

Rotational moulding is a widely used fabrication process for manufacturing hollow and large-size plastic products. Though researchers proved their hypothesis but were not able to prove the efficiency of the suggested techniques in the industrial field, which shows a big gap in heat transition of the rotomoulding process. Moreover, there is hardly any research has been conducted to analyse the heat flow in rotomoulding ovens where the duct has been considered as a heat transfer medium. However, the conclusions are already being studied by other researchers, but justifying theories through real-life implementation in the rotational moulding machine industrial arena is missing. Learning more about improved product results in terms of reduced manufacturing costs and carbon emissions will be beneficial. Based on empirical analysis of studies conducted over the past decade, enhancing the moulding area can lead to improved heat transfer. In addition to this, the authors of the review paper advise executing a thorough geometrical assessment of duct shapes and identifying insulating materials according to the oven configuration. The financial advantages of implementing ducts in ovens and utilising optimal insulation techniques demonstrate annual savings and energy reduction, alongside a declining trend in carbon emissions.

CRediT authorship contribution statement

Sutirtha Chowdhury: Writing – review & editing, Writing – original draft, Visualization, Formal analysis, Conceptualization. **Jayantha**

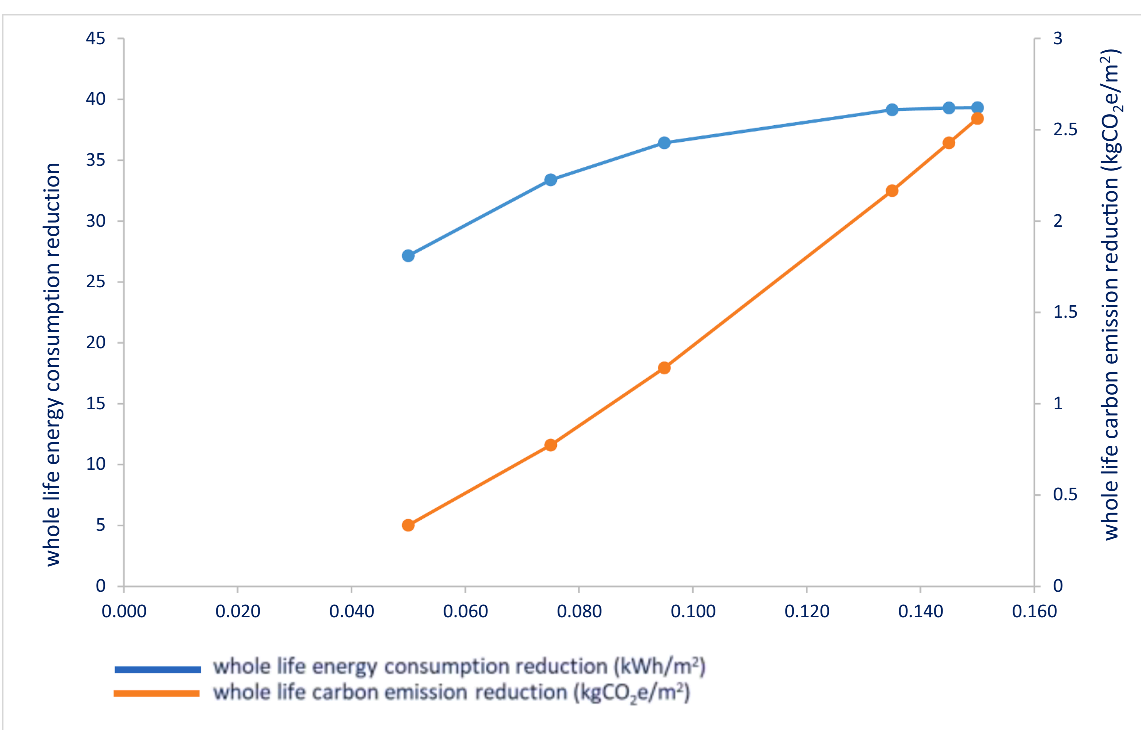

Fig. 23. Comparison of the reduction in whole-life energy and carbon consumption in relation to insulation thickness.

Epaarachchi: Writing – review & editing, Visualization, Supervision, Formal analysis, Conceptualization. **Ahmad Sharifian-Barforoush:** Writing – review & editing, Visualization, Supervision. **Md Mainul Islam:** Writing – review & editing, Visualization, Supervision.

Declaration of competing interest

The authors declare that they have no known competing financial interests or personal relationships that could have appeared to influence the work reported in this paper.

Data availability

Data will be made available on request.

References

[1] S. Rahner, The latest trend: rotational moulding, Kunststoffe Plast Europe (Germany) 88 (1998) 24–26.
[2] P. Nugent, Rotational molding. Applied Plastics Engineering Handbook: Processing and Materials, Elsevier, 2011, pp. 311–332, https://doi.org/10.1016/B978-1-4377-3514-7.10018-2.
[3] F.G. Torres, C.L. Aragon, Final product testing of rotational moulded natural fibre-reinforced polyethylene, Polym. Test. 25 (2006) 568–577, https://doi.org/10.1016/j.polymertesting.2006.03.010.
[4] S.J. Liu, K.H. Fu, Effect of enhancing fins on the heating/cooling efficiency of rotational molding and the molded product qualities, Polym. Test. 27 (2008) 209–220, https://doi.org/10.1016/j.polymertesting.2007.10.004.
[5] Ismail Sutaria, Rotational Molding Machine Market (2023). https://www.futuremarketinsights.com/reports/rotational-molding-machine-market. accessed June 28, 2024.
[6] L.M. Rincon-Rubio, B. Fayolle, L. Audouin, J. Verdu, A general solution of the closed-loop kinetic scheme for the thermal oxidation of polypropylene, Polym. Degrad. Stab. 74 (2001) 177–188, https://doi.org/10.1016/S0141-3910(01)00154-9.
[7] E. Richaud, F. Farcas, P. Bartoloméo, B. Fayolle, L. Audouin, J. Verdu, Effect of oxygen pressure on the oxidation kinetics of unstabilised polypropylene, Polym. Degrad. Stab. 91 (2006) 398–405, https://doi.org/10.1016/J.POLYMDEGRADSTAB.2005.04.043.
[8] S. Sarrabi, X. Colin, A. Tcharkhtchi, Kinetic modeling of polypropylene thermal oxidation during its processing by rotational molding, J. Appl. Polym. Sci. 118 (2010) 980–996, https://doi.org/10.1002/app.32459.
[9] G. Díaz, M. Sen, K.T. Yang, Effect of delay in thermal systems with long ducts, Int. J. Therm. Sci. 43 (2004) 249–254, https://doi.org/10.1016/J.IJTHERMALSCI.2003.07.004.
[10] K.O. Ogila, M. Shao, W. Yang, J. Tan, Rotational molding: a review of the models and materials, Express Polym. Lett. 11 (2017) 778–798, https://doi.org/10.3144/expresspolymlett.2017.75.
[11] K.K. Lim, A. Ianakiev, Modeling of rotational molding process: multi-layer slip-flow model, phase-change, and warpage, Polym. Eng. Sci. 46 (2006) 960–969, https://doi.org/10.1002/PEN.20481.
[12] K. Lim, A. Ianakiev, Two-dimensional slip-flow model of rotational moulding, (2004).
[13] K.K. Lim, A. Ianakiev, Numerical studies of the phase change and warpage under various process conditions for rotational molding, in: ANTEC… Conference Proceedings, Society of Plastics Engineers, 2004, pp. 897–901.
[14] A. Greco, Simulation of heat transfer during rotational molding, Wiley Online LibraryA Greco, A Maffezzoli, J VlachopoulosAdvances in Polymer Technology: Journal of the Polymer Processing, 2003, Wiley Online Library 22 (2003) 271–279, https://doi.org/10.1002/adv.10055.
[15] C. Bellehumeur, A. Medina, Dimensional stability of single-site ethylene copolymers in rotational molding, Wiley Online LibraryCT Bellehumeur, A Medina, H XuPolymer Engineering & Science, 2009, Wiley Online Library 49 (2009) 1400–1409, https://doi.org/10.1002/pen.21017.
[16] H. Xu, Modeling the morphology development of ethylene copolymers in rotational molding, Wiley Online LibraryH Xu, CT BellehumeurJournal of Applied Polymer Science, 2006, Wiley Online Library 102 (2006) 5903–5917, https://doi.org/10.1002/app.25092.
[17] H. Xu, Thermal residual stress development for semi-crystalline polymers in rotational molding, Wiley Online LibraryH Xu, CT BellehumeurPolymer Engineering & Science, 2008, Wiley Online Library 48 (2008) 283–291, https://doi.org/10.1002/pen.20887.
[18] A. Spence, The effect of processing variables on the formation and removal of bubbles in rotationally molded products, Wiley Online LibraryAG Spence, RJ CrawfordPolymer Engineering & Science, 1996, Wiley Online Library 36 (1996) 993–1009, https://doi.org/10.1002/pen.10487.
[19] R.J. Crawford, Rotational Moulding of Plastics, 1996 (No Title).
[20] A.G. Spence, R.J. Crawford, Removal of pinholes and bubbles from rotationally moulded products, Proc. Inst. Mech. Eng. B J Eng. Manuf. 210 (1996) 521–533, https://doi.org/10.1243/PIME_PROC_1996_210_151_02.
[21] R. Crawford, J.S.-P. and rubber processing and, undefined 1987, The formation and removal of gas bubbles in a rotational moulding grade of PE, Pascal-Francis. Inist. Fr (n.d.). https://pascal-francis.inist.fr/vibad/index.php?action=getRecordDetail&idt=7585550 (accessed July 7, 2024).
[22] M. Cramez, M. Oliveira, Optimisation of rotational moulding of polyethylene by predicting antioxidant consumption, ElsevierMC Cramez, MJ Oliveira, RJ Crawford. Polymer Degradation and Stability (2002). Elsevier (n.d.), https://www.sciencedirect.com/science/article/pii/S0141391001002348. accessed July 7, 2024.
[23] S. Bawiskar, Comparative study of warpage, global shrinkage, residual stresses, and mechanical behavior of rotationally molded parts produced from different polymers, Wiley Online LibraryS Bawiskar, JL WhitePolymer Engineering & Science, 1994, Wiley Online Library 34 (1994) 815–820, https://doi.org/10.1002/pen.760341006.
[24] R. Pop-Iliev, C.B. Park, K.H. Lee, The potentials for processing metallocene pe grades in rotational molding, in: Proceedings of PPS-18, International Conference of the Polymer Processing Society, Guimaraes, Portugal, 2002, p. 6.
[25] M. Kontopoulou, Bubble dissolution in molten polymers and its role in rotational molding, Wiley Online Library, M Kontopoulou, J VlachopoulosPolymer Engineering & Science, 1999, Wiley Online Library 39 (1999) 1189–1198, https://doi.org/10.1002/pen.11505.
[26] G.G.-P.E.& Science, undefined 2004, Bubble removal in rotational molding, Wiley Online LibraryG GogosPolymer Engineering & Science, 2004, Wiley Online Library 44 (2004) 388–394, https://doi.org/10.1002/pen.20035.
[27] S. Banerjee, Modeling of heat transfer in rotational molding, Wiley Online LibraryS Banerjee, W Yan, D Bhattacharyya, Polymer Engineering & Science, 2008, Wiley Online Library 48 (2008) 2188–2197, https://doi.org/10.1002/pen.21164.
[28] Laura Wood, Australian polyethylene Market growth insights, 2014-2024: blow moulding, pipe extrusion, film extrusion, rotational moulding, injection moulding - ResearchAndMarkets.Com, 2020.
[29] Australia Water Storage System Market Size, Share & Forecast 2029 | BlueWeave, (2023). https://www.blueweaveconsulting.com/report/australia-water-storage-system-market (accessed July 7, 2024).
[30] J.L. Throne, Opportunities for the next decade in blow molding: plastics processing technology: opportunities for the next decade, Plast. Eng. 54 (1998) 41–43.
[31] R.J. Crawford, Recent advances in the manufacture of plastic products by Rotomoulding (1996).
[32] C.A. Harper, Handbook of Plastic Processes, Wiley-Interscience, 2006.
[33] G. Gogos, X. Liu, L.O.-P.E.& Science, undefined 1999, Cycle time predictions for the rotational molding process with and without mold/part separation, Wiley Online LibraryG Gogos, X Liu, LG OlsonPolymer Engineering & Science, 1999•Wiley Online Library 39 (1999) 617–629. https://doi.org/10.1002/pen.11451.
[34] J. Fleischer, S. Koch, S.C.-P. Engineering, Manufacturing of Polygon Fiber Reinforced Plastic Profiles by Rotational Molding and Intrinsic Hybridization, Springer, 2015 n.d. https://link.springer.com/article/10.1007/s11740-015-0620-0. accessed July 7, 2024
[35] A. Greco, A. Maffezzoli, J. Vlachopoulos, Simulation of heat transfer during rotational molding, Adv. Polym. Tech. 22 (2003) 271–279, https://doi.org/10.1002/adv.10055.
[36] S. Bawiskar, J.L. White, Simulation of heat transfer and melting in rotational molding, Int. Polym. Proc. 10 (1995) 62–67, https://doi.org/10.3139/217.950062/HTML.
[37] R.J. Crawford, P. Nugent, Computer simulation of the rotational moulding process for plastics, Plastics Rubber Process. Appl. 11 (1989) 107–124.
[38] G. Gogos, L.G. Olson, X. Liu, V.R. Pasham, New models for rotational molding of plastics, Polym. Eng. Sci. 38 (1998) 1387–1398, https://doi.org/10.1002/PEN.10309.
[39] Reducing cycle times in rotational moulding of plastics: a theoretical and experimental analysis — Queen's University Belfast, (2004). https://pure.qub.ac.uk/en/studentTheses/reducing-cycle-times-in-rotational-moulding-of-plastics-a-theoret (accessed June 28, 2024).
[40] M.Z. Abdullah, S. Bickerton, D. Bhattacharyya, Rotational molding cycle time reduction through surface enhanced molds: part A - theoretical study, Polym. Eng. Sci. 47 (2007) 1406–1419, https://doi.org/10.1002/pen.20835.
[41] M.Z. Abdullah, S. Bickerton, D. Bhattacharyya, Rotational molding cycle time reduction through surface-enhanced molds, Part B: Experim. Study, Polym. Eng. Sci. 47 (2007) 1420–1429, https://doi.org/10.1002/PEN.20834.
[42] C. Ranganayakulu, X. Luo, S. Kabelac, The single-blow transient testing technique for offset and wavy fins of compact plate-fin heat exchangers, Appl. Therm. Eng. 111 (2017) 1588–1595, https://doi.org/10.1016/J.APPLTHERMALENG.2016.05.118.
[43] R. Gao, S. Chen, J. Zhao, Y. Zhang, A. Li, Coupling effect of ventilation duct bend with different shapes and sizes, Build. Simul. 9 (2016) 311–318, https://doi.org/10.1007/S12273-015-0267-Y/METRICS.
[44] B.L. Berrier, B.G. Allan, Experimental and computational evaluation of flush-mounted, S-duct inlets, AIAA Paper (2004) 8780–8792, https://doi.org/10.2514/6.2004-764.
[45] P. Spicka, M. Dias, Gas–liquid flow in a 2D column: comparison between experimental data and CFD modelling. ElsevierP Spicka, MM Dias, BL Jose'e Carloschemical Engineering Science, Elsevier, 2001, 2001(n.d.), https://www.sciencedirect.com/science/article/pii/S0009250901002767. accessed June 28, 2024.
[46] M. Onder, S. Sarac, E. Cevik, The influence of ventilation variables on the volume rate of airflow delivered to the face of long drivages, Tunnelling Underground Space Technol. 21 (2006) 568–574, https://doi.org/10.1016/J.TUST.2005.10.001.

[47] V.V. Agafonova, A.P. Skibin, V.Y. Volkov, Modeling of air distribution in an office building using microperforated textile air duct, IOP Conf. Ser. Mater. Sci. Eng. 1079 (2021) 052077, https://doi.org/10.1088/1757-899X/1079/5/052077.
[48] P. Raphe, H. Fellouah, S. Poncet, M. Ameur, Ventilation effectiveness of uniform and non-uniform perforated duct diffusers at office room, Build. Environ. 204 (2021) 108118, https://doi.org/10.1016/J.BUILDENV.2021.108118.
[49] K. Yang, T. Shi, T. Ming, Y. Wu, Y. Chen, Z. Yu, M.H. Ahmadi, K. Yang, T. Shi, T. Ming, Y. Wu, Y. Chen, Z. Yu, M.H. Ahmadi, Study of internal flow heat transfer characteristics of ejection-permeable FADS,, Energies 16 (2023) 4377, https://doi.org/10.3390/EN16114377, 2023, Vol. 16, 4377.
[50] M. Hekal, W.M. El-Maghlany, Y.A. Eldrainy, M. El-Adawy, Hydro-thermal performance of fabric air duct (FAD): experimental and CFD simulation assessments, Case Stud. Thermal Eng. 47 (2023), https://doi.org/10.1016/j.csite.2023.103107.
[51] J. Cai, G. Thierauf, Discrete optimization of structures using an improved penalty function method, Eng. Optim. 21 (1993) 293–306, https://doi.org/10.1080/03052159308940981.
[52] N.D. Kunabeva, A. Professor, Engineering and technology (A high impact factor, Int. J. Innovative Res. Sci. 6 (2017), https://doi.org/10.15680/IJIRSET.2017.0612075.
[53] S. Walunj, S. Shirsath, A. Biradar, A. Salvi, M. Deore, Study and analysis of air flow through duct, JETIR (2021). www.jetir.org.
[54] P. Wang, M. Yang, Z. Wang, Y. Zhang, A new heat transfer correlation for turbulent flow of air with variable properties in noncircular ducts, J. Heat Transfer 136 (2014), https://doi.org/10.1115/1.4027855/373220.
[55] Y. Zhang, M.M. Rahman, G. Chen, Development of k-R turbulence model for wall-bounded flows, Aerosp. Sci. Technol. 98 (2020), https://doi.org/10.1016/j.ast.2020.105681.
[56] T.T. Chandratilleke, R. Narayanaswamy, P. Wangdhamkoom, Convective heat transfer in airflow through a duct with wall thermal radiation, IOP Conf Ser Mater Sci Eng 10 (2010) 012026, https://doi.org/10.1088/1757-899X/10/1/012026.
[57] R. Narayanaswamy, A.J.C. King, T.T. Chandratilleke, Multimode heat transfer in an enclosure with multiple partitions, Australian J. Mech. Eng. 4 (2007) 87–92, https://doi.org/10.1080/14484846.2007.11464517.
[58] N. Ramesh, S.P. Venkateshan, Experimental study of natural convection in a square enclosure using differential interferometer, Int. J. Heat. Mass. Transf. 44 (2001) 1107–1117, https://doi.org/10.1016/S0017-9310(00)00170-8.
[59] N. Ramesh, W. Merzkirch, Combined convective and radiative heat transfer in side-vented open cavities, Int. J. Heat Fluid Flow 22 (2001) 180–187, https://doi.org/10.1016/S0142-727X(00)00080-1.
[60] N. Ramesh, C. Balaji, S.P. Venkateshan, An experimental study of natural convection and surface radiation in an open cavity, Int. J. Heat and Technology 19 (2001) 89–94.
[61] M. Schrittwieser, A. Marn, E. Farnleitner, G. Kastner, Numerical analysis of heat transfer and flow of stator duct models, IEEE Trans. Ind. Appl. 50 (2014) 226–233, https://doi.org/10.1109/TIA.2013.2267191.
[62] A. Boglietti, A. Cavagnino, D. Staton, M. Shanel, M. Mueller, C. Mejuto, Evolution and modern approaches for thermal analysis of electrical machines, IEEE Trans. Ind. Electron. 56 (2009) 871–882, https://doi.org/10.1109/TIE.2008.2011622.
[63] C. Kral, A. Haumer, M. Haigis, H. Lang, H. Kapeller, Comparison of a CFD analysis and a thermal equivalent circuit model of a TEFC induction machine with measurements, IEEE Trans. Energy Convers. 24 (2009) 809–818, https://doi.org/10.1109/TEC.2009.2025428.
[64] L.S. Sørensen, An introduction to Computational Fluid Dynamics: the Finite volume method, in: 1999. https://api.semanticscholar.org/CorpusID:146002756.
[65] CFD EXPERTS Simulate the Future, 2021.
[66] F.R. Menter, Two-equation eddy-viscosity turbulence models for engineering applications, AIAA J. 32 (1994) 1598–1605.
[67] A. Chaube, P.K. Sahoo, S.C. Solanki, Effect of roughness shape on heat transfer and flow friction characteristics of solar air heater with roughened absorber plate, WIT Trans. Eng. Sci. 53 (2006) 43–51, https://doi.org/10.2495/HT060051.
[68] W. Vieser, T. Esch, F. Menter, Heat transfer predictions using advanced two-equation turbulence models, ANSYS CFX Validation Report (2004) 1–62.
[69] H. Schlichting, K. Gersten, Boundary-layer theory, springer, 2016.
[70] T. Alam, R.P. Saini, J.S. Saini, Use of turbulators for heat transfer augmentation in an air duct – A review, Renew Energy 62 (2014) 689–715, https://doi.org/10.1016/J.RENENE.2013.08.024.
[71] G. Kalitzin, G. Medic, G. Iaccarino, P. Durbin, Near-wall behavior of RANS turbulence models and implications for wall functions, J. Comput. Phys. 204 (2005) 265–291, https://doi.org/10.1016/j.jcp.2004.10.018.
[72] D.L. Gee, R.L. Webb, Forced convection heat transfer in helically rib-roughened tubes, Int. J. Heat Mass Transf. 23 (1980) 1127–1136, https://doi.org/10.1016/0017-9310(80)90177-5.
[73] C. Thianpong, K. Yongsiri, K. Nanan, S. Eiamsa-ard, Thermal performance evaluation of heat exchangers fitted with twisted-ring turbulators, Int. Commun. Heat Mass Transfer 39 (2012) 861–868, https://doi.org/10.1016/J.ICHEATMASSTRANSFER.2012.04.004.
[74] T. Alam, R.P. Saini, J.S. Saini, Heat and flow characteristics of air heater ducts provided with turbulators—A review, Renew. Sustain. Energy Rev. 31 (2014) 289–304, https://doi.org/10.1016/J.RSER.2013.11.050.
[75] R.L. Webb, N.Y. Kim, Enhanced Heat Transfer, Taylor and Francis, NY, 2005.
[76] H. Ranjan, A.K. Bharti, M.S. Emani, J.P. Meyer, S.K. Saha, New combined heat transfer enhancement techniques used in laminar flow through non-circular ducts, Appl. Therm. Eng. 163 (2019) 114325, https://doi.org/10.1016/J.APPLTHERMALENG.2019.114325.
[77] S. Cai, Thermal Performance of Mechanical Pipe Insulation Systems at Below-Ambient Temperature, Oklahoma State University, 2013.
[78] V. Masatin, A. Volkova, A. Hlebnikov, E. Latosov, Improvement of district heating network energy efficiency by pipe insulation renovation with PUR foam shells, Energy Procedia 113 (2017) 265–269, https://doi.org/10.1016/J.EGYPRO.2017.04.064.
[79] S. Avikal, R. Devi, A.S. Bisht, K.C. Nithin Kumar, Design and thermal analysis of pipe insulation, Lecture Notes Mech. Eng. (2021) 455–465, https://doi.org/10.1007/978-981-16-0159-0_40/TABLES/2.
[80] A. Mittenbühler, J. Jung, Ceramic materials under high temperature heat transfer conditions, J. Nucl. Mater. 171 (1990) 54–62, https://doi.org/10.1016/0022-3115(90)90347-P.
[81] A. Keebaş, M. Ali Alkan, M. Bayhan, Thermo-economic analysis of pipe insulation for district heating piping systems, Appl. Therm. Eng. 31 (2011) 3929–3937, https://doi.org/10.1016/J.APPLTHERMALENG.2011.07.042.
[82] R. Levinson, W.W. Delp, D. Dickerhoff, M. Modera, Effects of airflow infiltration on the thermal performance of internally insulated ducts, Energy Build. 32 (2000) 345–354, https://doi.org/10.1016/S0378-7788(00)00055-4.
[83] M.S. Barkhad, B. Abu-Jdayil, M.Z. Iqbal, A.H.I. Mourad, Thermal insulation using biodegradable poly(lactic acid)/date pit composites, Constr. Build. Mater. 261 (2020) 120533, https://doi.org/10.1016/J.CONBUILDMAT.2020.120533.
[84] K.L. Wong, W.L. Chen, T.L. Hsien, H.M. Chou, The critical heat transfer characteristics of an insulated oval duct, Energy Convers. Manag. 51 (2010) 1442–1448, https://doi.org/10.1016/J.ENCONMAN.2010.01.019.
[85] O. Kaynakli, Economic thermal insulation thickness for pipes and ducts: a review study, Renew. Sustain. Energy Rev. 30 (2014) 184–194, https://doi.org/10.1016/J.RSER.2013.09.026.
[86] A. Bahadori, H.B. Vuthaluru, A simple method for the estimation of thermal insulation thickness, Appl. Energy 87 (2010) 613–619, https://doi.org/10.1016/J.APENERGY.2009.05.012.
[87] D. Kumar, S. Kumar, B.A. Bhayo, K. Harijan, M.A. Uqali, Economic and environmental impacts of thermal insulation used in different duct sizes, J. Thermal Eng. 6 (2020) 141–156, https://doi.org/10.18186/THERMAL.672085.
[88] X. Li, D.D. Tingley, A whole life, national approach to optimize the thickness of wall insulation, Renew. Sustain. Energy Rev. 174 (2023), https://doi.org/10.1016/j.rser.2022.113137.
[89] A quick reference guide for elected officials and staff whole-of-life costing, 2016.